Post-Hurricane Michael damage assessment using ADCIRC storm surge hindcast, image classification, and LiDAR

By

Joshua Davis[1], Diana Mitsova[2], Tynon C. Briggs[3], and Tiffany Roberts Briggs[3*]

1) Certified Floodplain Manager, Orlando, FL 32818

2) School of Regional and Urban Planning, Florida Atlantic University, 777 Glades Road, Boca Raton, FL 33431

3) Dept. of Geosciences, Florida Atlantic University, 777 Glades Road, Boca Raton, FL 33431

**Corresponding author: briggst@fau.edu*

ABSTRACT

Remote sensing data collected in the aftermath of a disaster can play a vital role in identifying badly damaged areas where homes and infrastructure have been destroyed, prioritizing emergency assistance needs, locating survivors, and providing restoration guidance. In this study, we use NOAA's National Geodetic Survey Emergency Response Imagery database, LIDAR, and tax appraiser data to assess storm damage after Hurricane Michael in Mexico Beach, FL. Post-Michael imagery was classified as debris, roofs, vegetation (trees and grass), sand, roads, and water. Pre-storm LiDAR-derived building footprints in the impacted area were overlaid on the reclassified post-storm imagery to quantify the extent of structural damage to residential areas. The extent of the damage was also examined using maximum wave height and depth of storm surge inundation derived from the output of the ADCIRC modeling system. Over 700 buildings were classified as considerably damaged or completely destroyed. The 2017 tax appraiser data were used to estimate the economic value of the storm impact. Results of this study may help in reconsidering existing building code requirements to protect people and property and reduce future storm damages.

ADDITIONAL KEYWORDS: Emergency response imagery, debris, supervised classification, surge modeling.

Manuscript submitted27 June 2019, revised & accepted 19 September 2019.

On October 10, 2018, Hurricane Michael made landfall in the Florida Panhandle between Mexico Beach and the Tyndall Air Force Base as a Category 5 storm with a sustained wind speed of 260 km/hr (160 mph) and a landfall pressure of 919 mbar (hPa) (Figure 1). Mexico Beach is a small coastal community in Bay County, Florida, with a population of just over 1,000 (US Census 2010). Hurricane Michael is considered to be one of the most powerful tropical cyclones and the second Category 5 hurricane (since Hurricane Andrew in 1992) to make landfall in the United States in recorded history. One of the most devastating impacts of Hurricane Michael was the destruction of a large number of residential and commercial structures. Multiple structures in Mexico Beach, Panama City, and other locations throughout the Florida Panhandle were leveled to the ground by high-end Category 5 hurricane winds or swept away by peak storm surges measured at 2.7 to 4.3 meters high (9 to 14 feet).

In addition to the extensive damage to property, Hurricane Michael caused extended power outages throughout the Florida Panhandle and parts of Georgia and Alabama. Data made available by the Florida Public Service Commission showed that over 95% of all accounts in 10 counties in the Florida Panhandle lost power after the hurricane made landfall (FPSC 2018). Extended power outages were recorded in several counties in the disaster area in the Florida Panhandle including Bay, Gulf, Gadsden, Jackson, Calhoun, and Washington counties. Additionally, data submitted by communications providers to the Disaster Information Reporting System (DIRS) of the Federal Communications Commission's (FCC) indicated that Hurricane Michael had a critical impact on communications services in the Florida Panhandle as well as parts of Georgia and Alabama (FCC 2019). Overall, 110 counties were part of the DIRS activation in the designated disaster area (FCC 2019). The power and communication blackouts made it difficult for first responders to conduct rapid damage assessments. Remote sensing data collected in the aftermath of a disaster can play a vital role in identifying badly damaged areas where homes and infrastructure have been destroyed, prioritizing emergency assistance needs, locating survivors, and providing restoration guidance.

Wind and water levels from tropical storms and hurricanes cause variable levels of damages to buildings and structures (Baradaranshoraka *et al.* 2017). Measured wind speeds are classified by the National Hurricane Center (NHC) based on the Saffir-Simpson hurricane wind scale (Simpson 1974). Measuring and predicting storm surge is more challenging, as water levels can be influenced by a number of factors in addition to wind speed, including storm size, intensity, forward speed, and distribution of wind speeds (Irish *et al.* 2008). Field-assessed surge levels are typically conducted by marking debris or water lines (Fritz *et al.* 2007). However, accurate determination of storm surge heights is critical to improving models of surge hazards (Resio *et al.* 2009). A number of studies integrate available data to reduce uncertainty in storm surge predications, such the advanced circulation (ADCIRC) model (Fleming 2008; Butler *et al.* 2012; Dietrich *et al.* 2012).

The need for rapid assessment of damages after natural disasters is critical to rescue, recovery, emergency management, and planning efforts. Remote sensing technologies, such as aerial imagery and airborne LiDAR, are commonly employed to determine post-disaster coastal change and flood damages (Zhang *et al.* 2005; Robertson *et al.* 2007; Stockdon *et al.* 2009), including to homes and infrastructure, and to prioritize emergency assistance (Meng *et al.* 2010, Macintosh 2013). Post-landfall damage analysis can also guide the restoration of basic infrastructure, identify

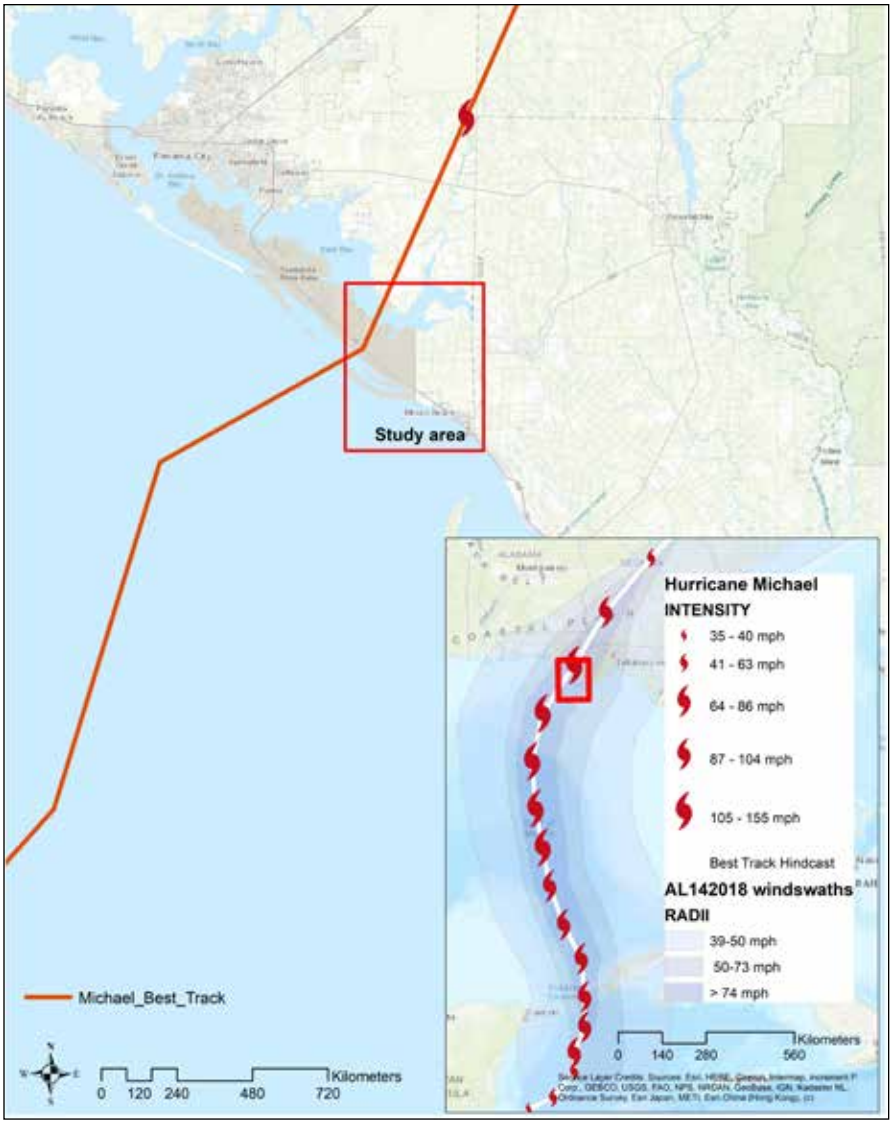

Figure 1. Location of the study area, where Category 5 Hurricane Michael made landfall near Tyndall Air Force Base and Mexico Beach, FL.

community vulnerability, and facilitate other post-disaster recovery operations (Gong and Maher 2014). Zhou and Gong (2018) employed remote sensing methods to determine component-level damage assessments for major building features such as walls, roofs, balconies, and structural supports due to Hurricane Sandy. As natural disasters become more frequent (van Aalst 2006), collecting time-critical information is imperative for determining recovery costs and reducing future risk (Kruse and Hochard 2019).

Reducing storm damage and community vulnerability will continue to require integration of current state-of-the-art technologies and improved model predictions that can inform hazard communication, building codes, and planning policies. This study focuses on the area near Hurricane Michael's landfall in Mexico Beach, FL (Figure 1). The objective is to assess post-Hurricane Michael damages using ADCIRC storm surge hindcast, image classification, and LiDAR. Six classes were chosen for classification of the post-Michael imagery: debris, roofs, vegetation (trees and grass), sand, roads, and water. Pre-storm LiDAR derived building footprints in the impacted area were overlaid on the post-storm imagery to quantify the extent of structural damage to the residential area. Hurricane damage to buildings were classified as "moderate" to "destroyed" based on post-storm aerial imagery. Finally, storm surge modelled using ADCIRC is overlain and compared to building damages.

MATERIALS AND METHODS

Data and data processing

The primary datasets used in this study were collected directly from government sources. Post-storm imagery was obtained from the National Geodetic Survey Emergency Response Imagery database operated by the National Oceanographic and Atmospheric Administration (NOAA). The database provides high resolution aerial imagery of extreme weather events from 2003 to the present. Hurricane Michael imagery from 11 October to 14 October was accessible as an online map service and available for direct download in either TIF or JPEG format. In this study, the assessment of the damages immediately following landfall was based on the 11 October Emergency Response Imagery dataset. Estimated sustained wind speed swaths (mph) based on preliminary HURDAT data from the National Hurricane Center (NHC) were downloaded as a web map and converted to shapefiles (NOAA-NWS 2018).

For comparison, the pre-disaster aerial imagery was obtained from the United States Geologic Survey (USGS) through the Earth Explorer website. Earth Explorer allows the user to search for data in a number of ways including adding a shapefile to the map to specify the search area. After a shapefile for the affected area was created in ArcMap, it was added to the search criteria in Earth Explorer for the area specified. For this project, the date range was set to one year prior to Hurricane Michael's landfall. The most comprehensive of the aerial imagery datasets available through Earth Explorer for the time period and the location was the National Agriculture Imagery Program (NAIP) GeoTIFF. The NAIP imagery is 1- meter or better in resolution, sufficient to reveal buildings and is available for the entire conterminous United States (USDA 2017).

Airborne LiDAR data were obtained through the USGS National Map service. The National Map allows for quick access to several products including LiDAR point clouds, geographic boundaries, hydrography, imagery and more. Raw LiDAR point data were collected for the affected area and downloaded for later processing as a LAS dataset into a Digital Elevation Model (DEM), a Digital Terrain Model (DTM), a Digital Surface Model (DSM, and a normalized Digital Surface Model (nDSM). Bare Earth DEMs, building footprints and tree coverage were derived from the LiDAR point cloud using Lidar Analyst™ (Textron Systems 2018).

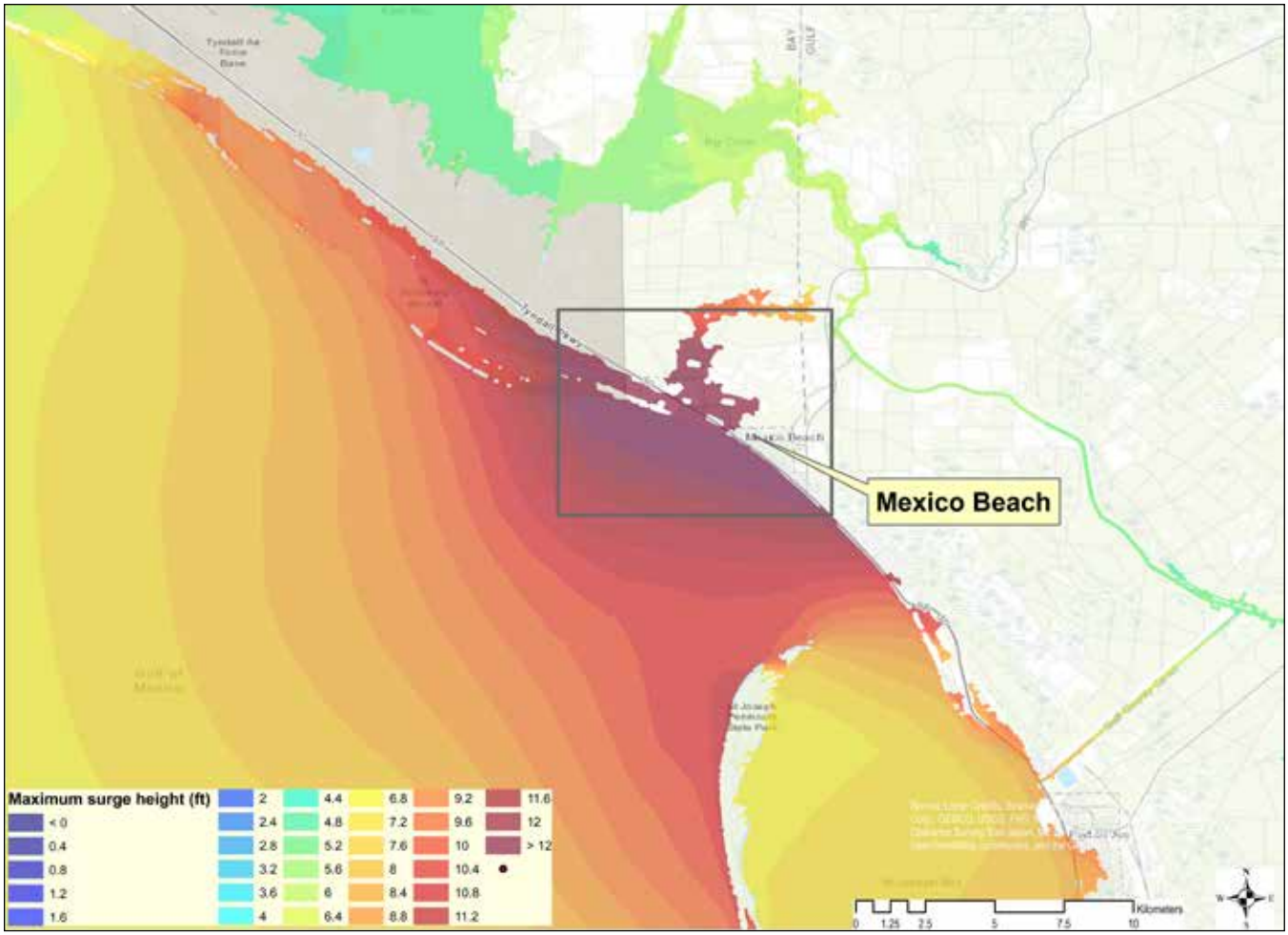

Figure 2. Hurricane Michael wind swaths obtained from NOAA and maximum ADCIRC-computed storm surge height.

METHODS

Wind and storm surge hindcast

Forecasts and hindcasts of hurricane storm surge and storm wave action are critical in the emergency response phase as they can facilitate mapping of flood-prone areas and assessment of the geographic extent of high water levels. In this analysis, we use the output of the ADvanced CIRCulation (ADCIRC) Coastal Circulation and Storm Surge Model obtained from the Coastal Emergency Risks Assessment (CERA) interactive Storm Surge Visualization tool (https://cera.coastalrisk.live) hosted by Louisiana State University (Losego *et al.* 2013). The tool was developed by the Coastal Hazards Center of Excellence at the University of North Carolina at Chapel Hill with support from the Department of Homeland Security (DHS) (Losego *et al.* 2013). ADCIRC utilizes the Generalized Wave Continuity Equation (GWCE) for computing water surface elevation (Luettich *et al.* 1992; Luettich and Westerink 2004). The model operates on a flexible unstructured mesh system with enhanced capabilities to vary resolution and simulate tide propagation over open ocean and on land using detailed topobathymetric information (Luettich *et al.* 1992; Luettich and Westerink 2004; Fleming *et al.* 2004; Dietrich *et al.* 2012; Dietrich *et al.* 2013; Dietrich *et al.* 2017). The use of an unstructured grid minimizes both local and global error by adjusting grid resolution to the solution gradient (Luettich *et al.* 1992; Luettich and Westerink 2004; Dietrich *et al.* 2013). In areas where solution gradients are large, ADCIRC supports high localized grid resolution whereas in areas with small solution gradients grid resolution is low (Luettich *et al.* 1992; Luettich and Westerink 2004; Dietrich *et al.* 2013). The ADCIRC modeling output includes storm surge height, inundation above ground, wind speed, significant wave height, and significant wave period (Luettich and Westerink 2004). ADCIRC computes storm surge as maximum water height or maximum inundation above ground (Luettich *et al.* 1992; Luettich and Westerink 2004; Losego *et al.* 2013). Maximum water levels and inundation depth indicate the highest modeled value at each grid point over the forecast or hindcast period (Losego *et al.* 2013). Possible storm surge water depth above ground is computed as the difference between local land elevation derived from LIDAR and compound water height above ground computed as the sum of tide level, storm surge height, and wave setup (Losego *et al.* 2013). Observed high water marks data for Bay and Gulf counties, Florida, were obtained from the USGS STN Flood Event database (https://stn.wim.usgs.gov/STNDataPortal/#). The STN peak surge data were compared with the CERA maximum water elevation points at the same location. All measured and simulated data were compiled in a single-source file (Table 1). The data were used to validate the storm surge heights generated by ADCIRC by calculating the root mean square error (RMSE).

Digital image analysis

The aerial imagery for both the pre-disaster and post-disaster datasets were compiled into two mosaic datasets. The first mosaic contained the NOAA post-disaster images, and the second contained

Table 1.
Comparison of USGS high-water mark data and ADCIRC-generated maximum water level heights.

High water mark Station ID	Ground elevation m	Ground elevation ft	USGS highwater mark m	USGS highwater mark ft	ADCIRC-computed storm surge height m	ADCIRC-computed storm surge height ft	Difference m	Difference ft
FLBAY27701	5.32	17.47	1.31	4.29	1.18	3.87	-0.13	-0.42
FLBAY27706	5.46	17.91	2.38	7.80	1.21	3.98	-1.16	-3.82
FLBAY27709	5.38	17.64	1.80	5.89	1.06	3.47	-0.74	-2.42
FLBAY27591	5.18	16.98	0.63	2.06	0.99	3.25	0.36	1.18
FLBAY27711	5.15	16.90	2.41	7.90	2.50	8.19	0.09	0.29
FLBAY27713	5.61	18.41	1.69	5.53	1.53	5.03	-0.15	-0.50
FLBAY27714	5.18	16.99	1.45	4.75	1.52	4.98	0.07	0.23
FLBAY27715	5.70	18.69	0.87	2.86	1.04	3.40	0.16	0.54
FLBAY27716	5.53	18.15	3.27	10.72	2.80	9.19	-0.47	-1.53
FLBAY27501	5.27	17.28	0.76	2.50	0.73	2.40	-0.03	-0.10
FLBAY27718	5.63	18.46	1.33	4.37	0.86	2.83	-0.47	-1.54
FLBAY27720	5.11	16.78	2.01	6.59	0.72	2.35	-1.29	-4.24
FLBAY27659	4.40	14.45	0.78	2.57	0.66	2.15	-0.13	-0.42
FLBAY27657	4.03	13.22	0.59	1.94	0.38	1.24	-0.21	-0.70
FLGUL27670	5.03	16.50	0.59	1.92	0.48	1.56	-0.11	-0.36

images from 2017 for the same location. In an effort to differentiate the land cover pre- and post-Hurricane Michael, a supervised classification method via the maximum-likelihood algorithm was run through ESRI's ArcMap 10.6.1 software. The maximum likelihood algorithm is one of the most frequently utilized classification methods in remote sensing applications (Lu *et al.* 2013; Rawat *et al.* 2015). This classification method is heavily weighted upon the probability that a pixel within the image data belongs to a specific class (Rawat and Kumar 2015). The computation time needed to carry out this method is significant due to the algorithms consideration of class variability by using the covariance matrix and as with most statistical analysis, a greater number of samples would reduce this error.

The two sets of aerial imagery were reclassified using the method described in Price (2010), which employs supervised classification based on the spectral signatures of a set of features of interest. Seven classes were chosen for classification of the post-Michael imagery including *construction and demolition debris*, *roofs*, *grass (non woody vegetation)*, *trees, sand*, *roads*, and *water*. Each class was trained using the Image Classification Toolbar Training Sample Manager in ArcGIS. Proper spectral training sample datasets were pivotal to the methodology employed in this study. Successful maximum likelihood is heavily dependent upon adequate spectral training sample datasets to teach the algorithm how to build accurate relationships as well as set clearly defined boundaries amongst various classes for reliable classification. Since each training sample is presumed to be normally distributed, the classes for this study were created with the most robust training sample dataset possible for both the pre- and post-storm land cover classifications. Due to the extensive size of the training sample datasets used, slight over-classification of particular groups such as water was observed in the final output. Fortunately, the model performed well classifying the groups of chief concern, including buildings, debris, and accessible roads. Roadways, sandy or bare earth areas, debris fields, and building roofs were clearly defined and situated as expected in comparison to the Mexico Beach aerial imagery utilized.

Table 2.
Building damage classification.

Damage state	Damage factor range (%)	Control damage factor (%)
1 — Moderate	10-30	20
2 — Heavy	30-60	45
3 — Major	60-100	80
4 — Destroyed	100	100

Housing damage assessment

Although the digital image analysis provides information about the extent of the overall post-landfall impact, it does not provide sufficient detail to quantify damage to structures. Building footprints and tree coverage were derived from the LiDAR point cloud using Lidar Analyst™ (Textron Systems 2018) and overlaid on the post-disaster imagery to estimate the total number of damaged buildings as well as the level of damage. A classification scheme describing the damage state of buildings in Mexico Beach, FL, post-Hurricane Michael was developed. A modified damage probability matrix was created based on how FEMA classifies earthquake damage (FEMA 1998). Each building footprint was given a single point to identify the location and classify the damage state of the structure. Minor damage could not be identified or classified using the available ortho-imagery and pixel-based image analysis approach (Ramlal *et al.* 2018), and was therefore omitted from the analysis. Therefore, the study focused on the following four categories: (1) *moderate*: significant damage to structures within the parcel warranting repair; (2) *heavy*: extensive damage to structures within the parcel requiring major repairs; (3) *major*: lack of roofing, localized debris within the parcel, and downed trees; and (4) *destroyed*: total destruction of the once erect structure within the parcel. The building damage state classification is given within a range of damage factor and control damage factors (Table 2). A hotspot analysis using the Getis-Ord G_i^* test statistic (Getis and Ord, 1992) was conducted to identify the areas with the highest concentration of heavily damaged or destroyed buildings. A high positive z-score and low p-value of the Getis-Ord G_i^* local test statistics indicate a significant spatial clustering or a hotspot (Getis and Ord, 1992). Overall, higher positive z-scores suggest more

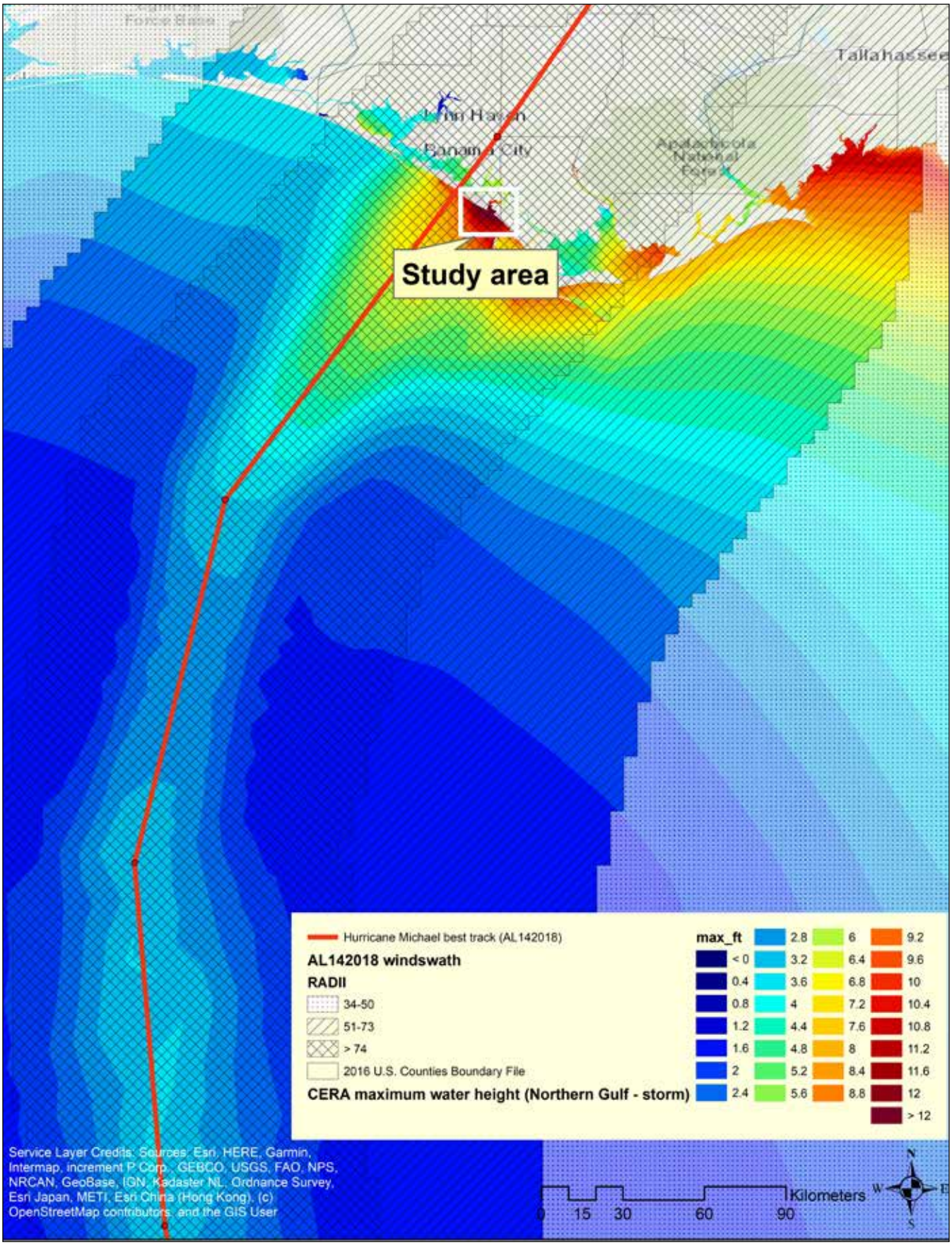

Figure 3. Maximum ADCIRC-computed water levels on the SL16v31 mesh for the NHC best-track analysis.

Figure 4. Mexico Beach area devastated by Hurricane Michael: (a) post-hurricane Michael disaster area; (b) pre-hurricane (2017) image of the area; and (c) comparison using the *swipe* tool to overlay before and after images.

intense clustering. Tax appraiser data were used to estimate the value of the extensively damaged property.

RESULTS

Hurricane Michael storm surge hindcast and water levels above ground

Hurricane Michael intensified to a Category 5 storm shortly before making a landfall, and maintained its intensity nearly 130 km (80 mi) further inland with observed wind gusts of 185 km/h (115 mph) (NWS 2018). Hurricane Michael's wind swaths and the maximum ADCIRC-computed storm surge water levels illustrate the damaging conditions experienced in Mexico Beach (Figure 2).

More detailed modeled storm-induced extreme (98% exceedance) water levels at Mexico Beach following Hurricane Michael show that the storm caused peak storm surge inundation of 2.7-4.2 m (9-14 ft) between the City of Mexico Beach and Indian Pass (Figure 3). Large waves and high winds caused severe erosion of the beach leading to complete destruction of the Mexico Beach pier and several buildings. The extent of the devastation within the western portion of Mexico Beach before and after landfall of Hurricane Michael can be easily recognized as a contrast between the pre-disaster images from 2017 and the post-hurricane impact (Figure 4). Using the *swipe* tool in the *Effects* toolbar in ArcMap shows the difference between the images in real time and can be useful in identifying properties that have been affected by the hurricane. The destruction of multiple structures by storm surge and high winds led to a large amount of debris and sand that were transported further inland covering roadways and obstructing emergency response operations.

An objective evaluation of the CERA storm surge data were conducted using peak surge values in the Mexico Beach area. Observed high water marks data were obtained from 15 USGS STN Flood Event stations and compared to the ADCIRC-computed maximum storm surge water level heights (Table 2). The results indicate that ADCIRC simulation slightly underestimates peak storm surge in most locations with larger estimated differences in the eastern portion of the study area. The resulting RMSE of 0.5 m (1.75 ft) indicates that there is an acceptable level of agreement between the two datasets.

Image classification to identify debris fields and sediment deposition

Initially, ten samples of each class were taken by drawing a polygon over where a representative of the class appeared in the image. Subsequently, additional signature samples were collected. The training sample size for the *roof* signature was increased to 100. In total, 50 training samples were collected for the *vegetation* class and 25 training samples were assigned to the *water* class. The three remaining classes — roads, debris, and sand — were each given 100 training samples assuming that a more robust sample of the various classes would increase the output resolution. Once the samples were chosen, they were converted into a signature file (Price 2010). The next step in the process was to use the maximum likelihood classification tool, specifying the clipped mosaic image as the input, setting the *a priori* weighting to equal, and setting the signatures file as the input signatures. The resulting classified raster shows *water* in blue, *trees* in dark green, *sand* in beige, *roof*

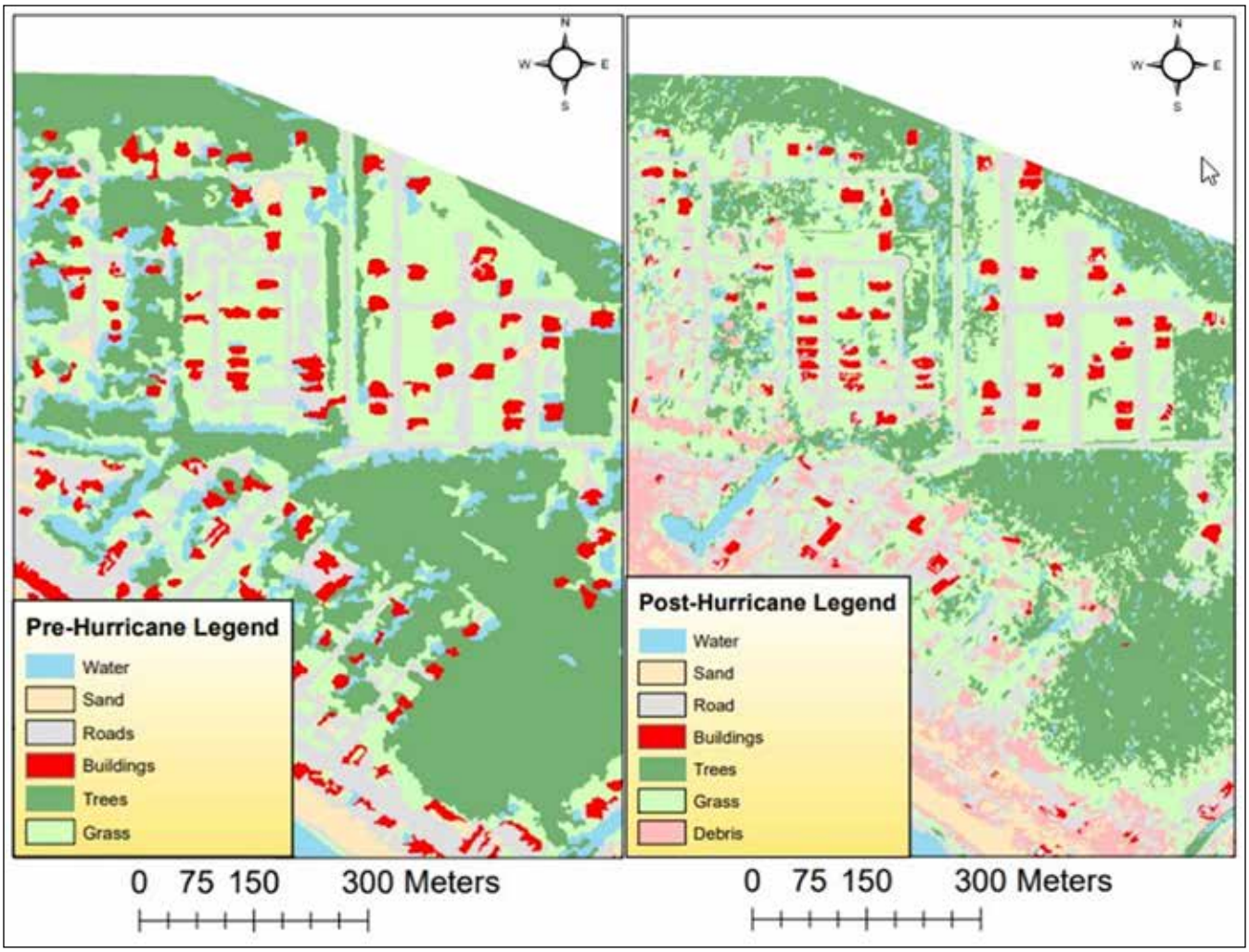

Figure 5. Maximum likelihood classification of Mexico Beach area for pre- and post-Hurricane Michael landfall showing the hurricane-induced change.

in red, *road* in grey, *grass* in light green, and *debris* in rose. The processes were then repeated for the 2017 pre-hurricane Michael imagery omitting the *debris* class. The procedure from (Mattupalli *et al.* 2018) was followed for all post-processing of classified images. The majority filter tool was used to smooth out the jagged edges and obtain more continuous feature boundary lines (Price 2010). The resulting shapefile contained less isolated pixels and was run through the boundary clean tool to find groups of values with the most pixels and give priority to these bigger groups for further smoothing. The final post-classification generalization tool was the nibble tool. With this tool a mask was overlain on the input raster data specifying that small pixel clusters where replaced by the value of the closest pixel within Euclidian distance.

The immediate post-storm imagery (one day) following Hurricane Michael's landfall near the City of Mexico Beach, FL, provided the opportunity for rapid assessment of the community devastation. Pooling water and sand deposition (i.e. overwash) tens of meters inland from the beach-dune systems were identified from the post-storm imagery illustrating the extent of inundation from storm surge (Figure 5). Overwash occurred across nearly the entire beach-dune system at Mexico Beach, with approximately 3.9 km (2.4 mi) of beach-dune vegetation lost due to burial or simply uprooted. The apparent storm-induced erosion and damage to the coastal vegetation likely lead to the higher degree of obstructed roadways and damaged seaside infrastructure (Figure 5).

Misclassification of certain classes occurred despite the high spatial resolution of the red, green, and blue (RGB) imagery (Mattupalli *et al.* 2018). Changes in water color and turbulence in the post storm imagery (particularly in breaking waves, small canals, waterways, creeks and forested areas) caused the spectral properties to more closely resemble the *grass* or *tree* classes. This is due to the spectral signatures of vegetation having the highest reflectance at the green bands in contrast to water which has very low reflectance across all RGB bands (Parece and Campbell 2015; Zakaluk and Ranjan 2008). Another factor that affected the land cover classification accuracy was the presence of shadows in the imagery. It is well-founded that shadows cause uncertainty in the interpretation and analysis of remotely sensed imagery (Bauer and Wu 2013; Zakaluk and Ranjan 2008).

Housing damage assessment

Assessment of initial damage to homes in Mexico Beach, FL, following the landfall of Hurricane Michael was conducted using photo-interpretation of a set of damage classes based on the damage factor ranges (in percent) identified in Table 2. The results (Table 3) indicate that 732 structures in the study area suffered moderate to severe damage. Among those, 355 residential, commercial, and institutional buildings structures were

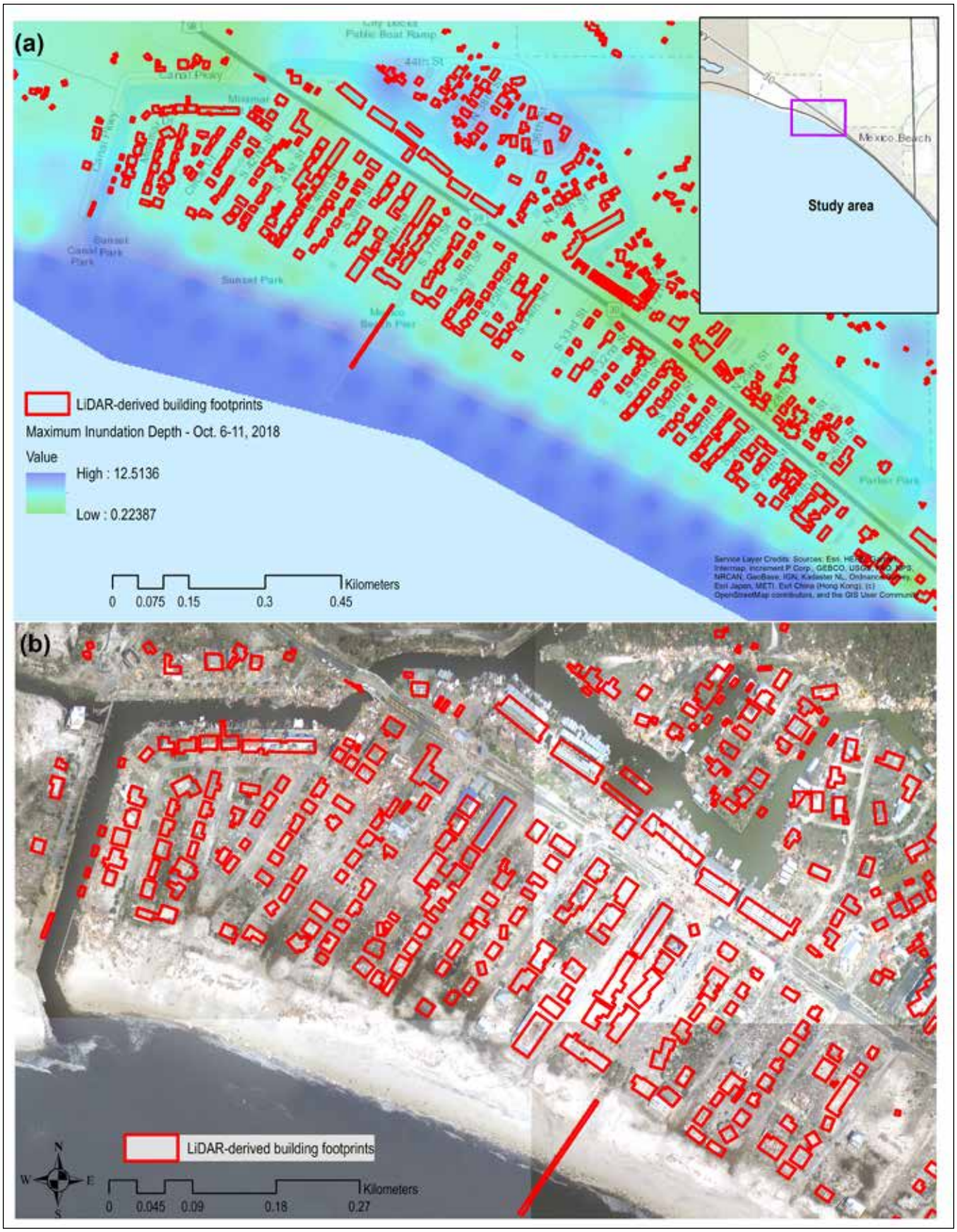

Figure 6. Property damage caused by Hurricane Michael near Mexico Beach: (a) maximum inundation depth based on Hurricane Michael hindcast using NHC's best track (gray colors indicate regions that were not wetted within the ADCIRC simulation); (b) aerial imagery of the devastation caused by the hurricane.

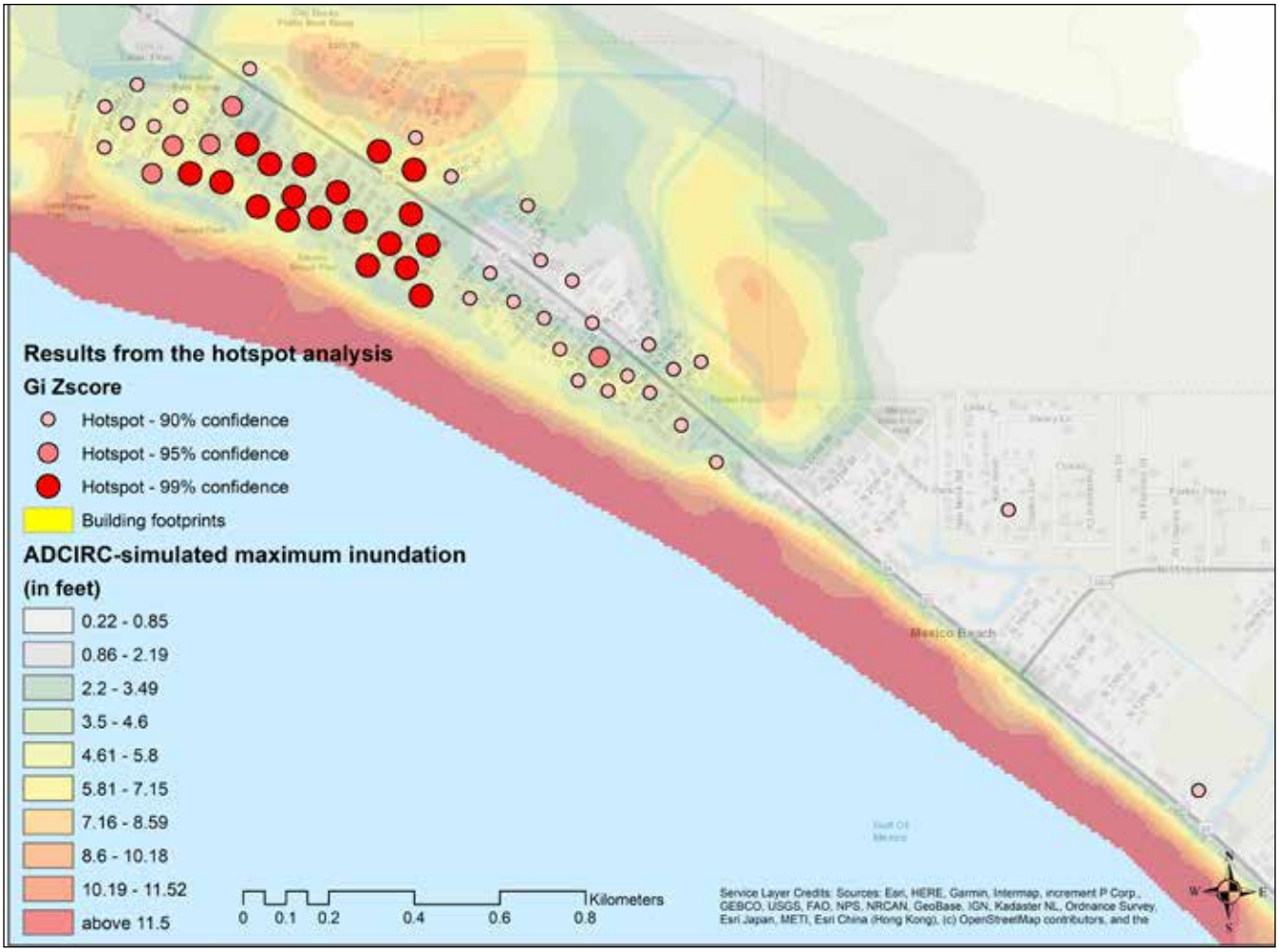

Figure 7. An overlay of the ADCIRC-simulated maximum inundation and the results of the hotspot analysis indicate that most of the destruction occurred in the areas severely affected by storm surge (the hotspot analysis is based on a 30-m [100-ft] search radius).

extensively damaged. Most of the impacted structures were single family homes. Based on the photo-interpretation of damage, 281 homes were identified as reduced to rubble or bare foundation slabs and 167 with major damages. Additionally, 112 homes suffered heavy to moderate damage warranting considerable repair. According to the 2017 tax appraisal data, the total assessed value of the affected structures amounts to $118,663,321. At least 52 multi-family structures also suffered severe damages. The analysis also suggests that 73 mobile homes were extensively damaged (24 of them were completely destroyed and 29 suffered major damages). The findings indicate that local businesses suffered comparable level of damage and destruction including hotels, motels, restaurants, financial institutions, office buildings, and warehouses.

The highest percentage of damaged structures occurred in the western part of the study area. Overall, from a total of 476 structures in the area, 379 were severely damaged (79.6%). Figure 6 shows an overlay of the post-Hurricane Michael landfall aerial imagery with the maximum inundation depth simulated by ADCIRC (based on Hurricane Michael hindcast using NHC's best track). A hotspot analysis of the damages indicate that a high proportion of the extensively damaged structures occur in the area most affected by storm surge. The z-scores resulting from computing the Getis-Ord Gi* test statistic were reclassified to represent hotspots at 90%, 95%, and 99% confidence levels (Figure 7).

DISCUSSION

Hurricane-force winds, storm surge, and flooding create multiple risk factors that can threaten property and infrastructure (Adams *et al.* 2010). In the aftermath of a disaster, especially when infrastructure services such as power and communications are disrupted, emergency response photogrammetry can provide valuable information needed to conduct damage assessments. This study used NOAA's Emergency Response Imagery database, LiDAR, and tax appraiser's data to conduct an assessment of the devastation inflicted by Hurricane Michael in and around the City of Mexico Beach, FL. Over 700 buildings in the area were identified as extensively damaged by the hurricane using visual reconnaissance and classification of damage. Using traditional aerial imagery taken at nadir (when the camera axis is perpendicular to the object on the ground) has advantages in identifying roof damage (which is a common indicator of high winds) but has limitations when damages result from storm surge and flooding (Adams *et al.* 2010, Li *et al.* 2019). To this respect, this study has certain limitations as it may have underestimated the extent of the damages to the building stock.

Using both ADCIRC-simulated storm surge and image classification, debris and sediment deposition analyses were conducted using supervised image

Table 3.
Total number of structures in Mexico Beach affected by Hurricane Michael by use, damage state, and assessed cumulative value using 2017 tax appraisal data.

Use description	Damage state (number of structures) Destroyed	Major	Heavy	Moderate	Total number of structures	Assessed cumulative value of heavily damaged structures
Camps	1				1	$1,223,653
Churches	1	1		1	3	$1,009,131
Condominiums	2	2			4	$987,405
Financial institutions (banks, savings and loan companies, mortgage companies, credit services)		1			1	$392,308
Hotels, motels	1	7			8	$6,986,062
Mobile homes	24	29	12	8	73	$5,297,970
Multi-family (10 units or more)	11	6		3	20	$3,068,407
Multi-family (fewer than 10)	22	13	1		36	$8,257,826
Municipal, other than parks, recreational areas, colleges, hospitals	1	3			4	$3,359,883
Office buildings, non-professional service buildings, one-story	2				2	$542,171
Parking lots (commercial or patron), mobile home parks		1			1	$1,281,947
Residential (common elements / areas)		4	1		5	$510,494
Restaurants, cafeterias	3		1		4	$810,339
Single family	281	167	30	82	560	$118,663,321
Stores, one-story	1	1			2	$388,932
Other commercial	4	1			5	$1,098,615
Other governmental	1				1	$162,448
Warehousing, distribution terminals, trucking terminals, van and storage warehousing		1		1	2	$649,966
Total	**355**	**237**	**45**	**95**	**732**	**$154,690,867**

classification. These analyses provided further background information for the damage analysis. The hotpot analysis of extensively damaged buildings confirmed that a large proportion of the damages (over 50%) occurred in the western part of the City of Mexico Beach which also overlaps with the area where maximum inundation levels were computed based on the ADCIRC-derived storm surge hindcast. Although model validation analysis revealed that ADCIRC slightly underestimated observed storm surge elevations, there was an overall agreement between storm surge inundation, sand and debris fields, and damage extent and severity. The entire area of Mexico Beach was impacted by the strong hurricane-induced winds. As expected, higher damages correspond to the region of higher onshore wind velocity and associated storm surge in the northeast quadrant of the storm and storm path. In addition, the hotspot analysis reveals higher damages in the western part of the study area, where the surge inundation inland was greater. A greater density of building damages in this area due to surge inundation is due to the lower land elevation, as compared to the area situated ~2 meters higher along a coastal ridge further east (Figure 8). Post-hurricane reconnaissance can be further improved with the use of unmanned aerial vehicles (UAVs) (Adams *et al.* 2010). UAVs provide capabilities for collecting digital imagery at an oblique angle that can display additional details of damage undetectable from a nadir perspective (Adams *et al.* 2010).

Damage assessments can play a critical role in disaster recovery planning and improving community resilience (Meyer and Hendricks 2018). While Florida is known nationally for upholding some of the most stringent building codes, there are regional differences in some requirements due to lower probability of a hurricane strike based on existing storm history records (Viglucci et al. 2018). According to the Building Code Wind Maps developed by the Florida Division of Business and Professional Regulation, the area of landfall in Mexico Beach has comparatively less stringent wind requirements (209 km/h or 130 mph) compared to other areas of Florida. Coastal areas in southwest and southeast Florida are required to build to design wind speeds of 260km/h (160 mph) (FDBPR 2014). The difference is related to fewer direct hurricane strikes historically in the Mexico Beach area, with only seven in existing records dating back to 1900 (NHC 2019). FDBPR (2014) uses wind speeds corresponding to approximately a 15% probability of exceedance in 50 years with an annual exceedance probability of less than 0.3%. As a comparison, Sarasota County has enforced more stringent wind requirements of 240 km/h (150 mph), despite having a similar number of historical hurricane strikes between 1900 and 2010 as Bay County (NHC 2019). As the area prepares to rebuild, reconsideration of existing building code requirements and enforcement of stricter strength, load and resistance factor designed to protect people and property could reduce future exposure of local communities to high wind and surge damage.

CONCLUSIONS

This study employed NOAA's National Geodetic Survey Emergency Response

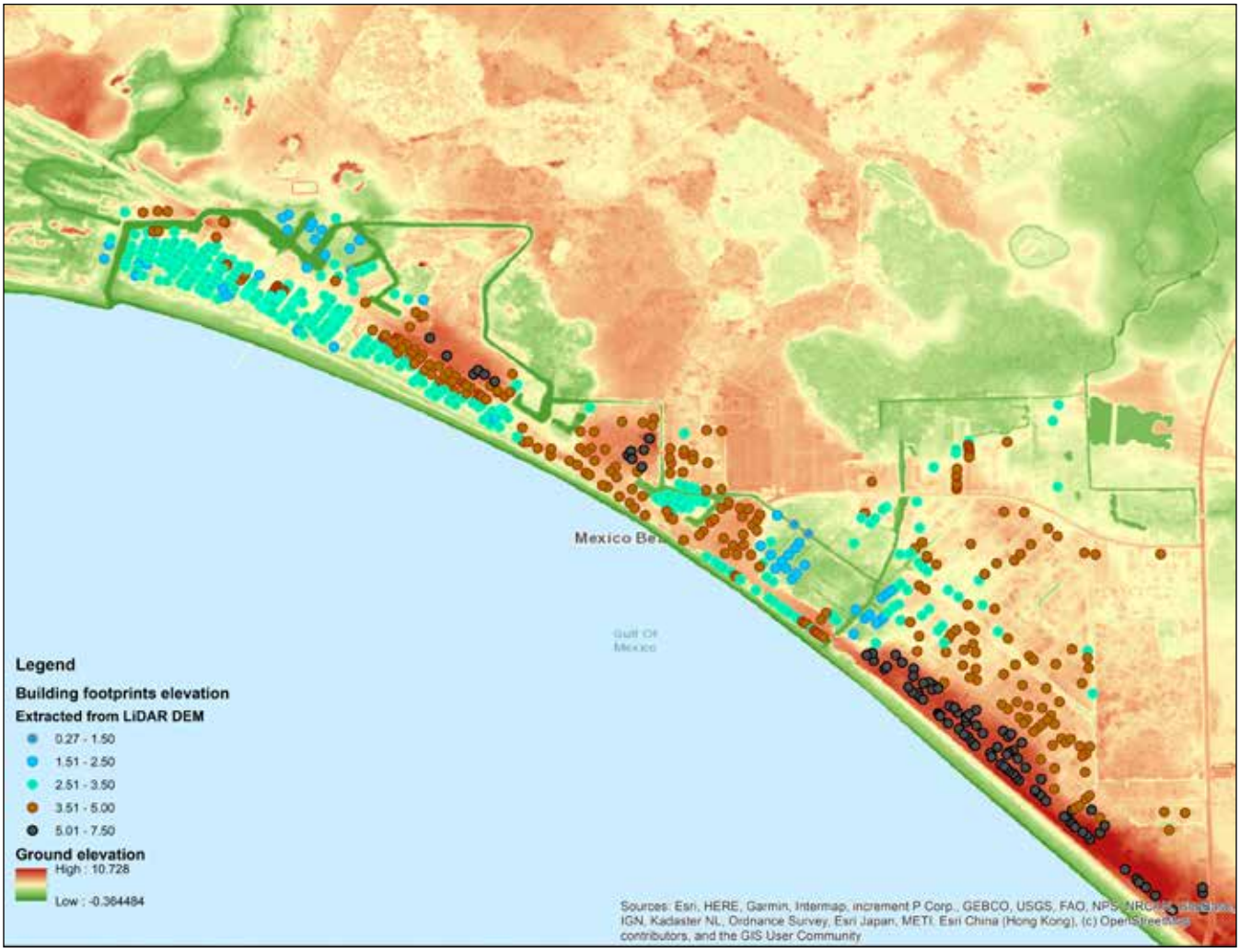

Figure 8. Building footprint elevations extracted from LiDAR DEM (value to points) in relation to ground elevation. The northwest section of the study area where most of the destruction occurred lies at elevations below 3 ft. The areas to the southeast are located along a coastal ridge with ground elevations between 5 and 7.5 ft.

Imagery database, LIDAR, and tax appraiser data to assess storm damage in Mexico Beach, Florida after Category 5 Hurricane Michael made landfall nearby. In the Mexico Beach area, more than 700 buildings were classified as either considerably damaged or completely damaged. Many of these structures were single family homes. The highest percentage of damaged structures occurred in the western part of the study area. In addition, debris and sand were transported inland and deposited on roadways, with overwash of nearly the entire beach-dune system of Mexico Beach.

An independent hotspot analysis of structural damages compared with maximum wave height and depth of storm surge inundation both revealed a higher proportion of extensive damage along the lower-lying western portion of the study area, with nearly 80% determined to be severely damaged. Based on a comparison of the ADCIRC simulation with USGS high water mark data, ADCIRC slightly underestimated peak storm surge inundation in the eastern portion of the study area. The total assessed value of the structures damaged in Mexico Beach due to Hurricane Michael were estimated at $118,663,321.

Results of this study could help improve disaster response, recovery, and planning, as well as improve community resilience. As communities rebuild after such natural disasters, reconsideration of existing building code requirements may reduce future risk to people and property. Future efforts in prioritizing emergency response efforts and restoration guidance may benefit from the use of remote sensing data to rapidly assess storm damages.

ACKNOWLEDGEMENTS

This article is based on research supported by the U.S. National Science Foundation Grant CMMI#1541089. Any opinions, findings, conclusions or recommendations expressed here are those of the authors and do not necessarily reflect the views of the National Science Foundation.

REFERENCES

Adams, S., Friedland, C., and M. Levitan, 2010. "Unmanned aerial vehicle data acquisition for damage assessment in hurricane events." *Proc.8th International Workshop on Remote Sensing for Disaster Management*, Tokyo, Japan, Vol. 30, Retrieved from: https://pdfs.semanticscholar.org/20bd/e467b925594bf6c40d09012120af42d6d4d8.pdf.

Baradaranshoraka, M., Pinelli, J-P., Gurley, K., Peng, X., and M. Zhao, 2017. "Hurricane wind versus storm surge damage in the context of a risk prediction model." *J. Structural Eng.* 143(9), 04017103, American Society of Civil Engineers.

Bauer, M.E., and J. Wu., 2013. "Evaluating the effects of shadow detection on QuickBird image classification and spectroradiometric restoration." *Remote Sensing*, 9, 4450.

Butler, T., Altaf, M.U., Dawson, C., Hoteit, I., Luo, X., and T. Mayo, 2012. "Data assimilation within the Advanced Circulation (ADCIRC) mod-

eling framework for hurricane storm surge forecasting." *Monthly Weather Review* 140, American Meteorological Society, 2215-2231.

Dietrich, J.C., Tanaka, S., Westerink, J.J., Dawson, C.N., Luettich Jr., R.A., Zijlema, M., Holthuijsen, L.H., Smith, J.M., Westerink, L.G., and H.J. Westerink, 2012. "Performance of the unstructured-mesh, SWAN+ADCIRC model in computing hurricane waves and surge." *J. Scientific Computation* 52, 468-497.

Dietrich, J.C., Dawson, C.N., Proft, J.M., Howard, M.T., Wells, G., Fleming, J.G., Luettich Jr., R.A., Westerink, J.J., Cobell, Z., Vitse, M., Lander, H., Blanton, B.O., Szpilka, C.M., and J.H. Atkinson, 2013. "Real-time forecasting and visualization of hurricane waves and storm surge using SWAN+ADCIRC and FigureGen." In: Dawson, C. and Gerritsen, M. (eds.), *Computational Challenges in the Geosciences*, The IMA Volumes in Mathematics and its Applications 156, DOI 10.1007/978-1-4614-7434-0 3, 49-70, © Springer Science+Business Media New York.

Dietrich, J.C., A. Muhammad, M. Curcic, A. Fathi, C.N. Dawson, S.S. Chen, and R.A. Luettich Jr., 2017. "Sensitivity of storm surge predictions to atmospheric forcing during Hurricane Issac". *J. Waterway, Port, Coastal, Ocean Engineering*, 144(1): 04017035. DOI: 10.1061/(ASCE) WW.1943-5460.0000419.

Federal Communications Commission (FCC), 2019. "October 2018 Hurricane Michael's impact on communications: preparation, effect, and recovery." A Report of the Public Safety and Homeland Security Bureau, Public Safety Docket No. 18-339. Retrieved from: https://www.fcc.gov/document/fcc-releases-report-communication-impacts-hurricane-michael.

Federal Emergency Management Agency (FEMA), 1998. "Estimating losses from future earthquakes." [microform]: (panel report and technical background) / Panel on Earthquake Loss Estimation Methodology, Committee on Earthquake Engineering, Commission on Engineering and Technical Systems, National Research Council. (1998). Washington, DC.

Fleming, J., Fulcher, C., Luettich Jr., R.A., Estrade, B., Allen, G., and H. Winer, 2008. "A real time storm surge forecasting system using ADCIRC." M.L. Spaulding (Ed.), *Proc. Estuarine and Coastal Modeling X*, ASCE (2008), 373-392.

Florida Division of Business and Professional Regulation (FDBPR), 2014. "2014 Florida Building Code Wind Maps." Retrieved from: http://www.floridabuilding.org/fbc/Wind_2014/2014_Wind_Maps.htm.

Florida Public Service Commission (FPSC), 2018. "Hurricane Season Power Outage Reports." Retrieved from: http://floridapsc.com/Home/HurricaneReport.

Fritz, H.M., Blount, C., Sokoloski, R., Singleton, J., Fuggle, A., McAdoo, B.G., Moore, A., Grass, C., and B. Tate, 2007. "Hurricane Katrina storm surge distribution and field observations on the Mississippi barrier Islands." *Estuarine, Coastal and Shelf Science* 74, 12-20.

Getis, A., and J.K. Ord, 1992. "The analysis of spatial association by use of distance statistics." *Geographic Analysis* 24(3), 189-206.

Gong, J., and A. Maher, 2014. "Use of mobile LiDAR data to assess hurricane damage and visualize community vulnerability." *Transportation Research Record: Journal of the Transportation Research Board,* No. 2459, Transportation Research Board of the National Academies, Washington DC, 119-126.

Irish, J.L., Resio, D.T., and J.J. Ratcliff, 2008. "The influence of storm size on hurricane surge." *J. Physical Oceanography* 38, 2003-2013

Kruse, J., and J. Hochard, 2019. "Economics, insurance, and flood hazards." *Southern Economic Journal* 85(4), 1027-1031.

Li, Y., Hu, W., Dong, H., and X. Zhang, 2019. "Building damage detection from post-event aerial imagery using single shot multibox detector." *Applied Sciences, 9*, 1128.

Losego, J., Luettich, R.A., Kaiser, C., Blanton, B., and J. Fleming, 2013. "CERA-Atlantic storm surge web page: improvements for 2013 based on EM feedback." Coastal Hazards Center, University of North Carolina at Chapel Hill. URL: https://www.ecu.edu/renci/HurricaneWorkshop/2013HurricaneWorkshop/Losego_CERA.pdf

Lu, D., Mausel, P., Batistella, M., and Moran, E. 2013. "Comparison of land-cover classification methods in the Brazilian Amazon basin." *Photogrammetric Engineering and Remote Sensing* 70(6), 723-731.

Luettich, R.A., Jr., J.J. Westerink, and N.W. Scheffner, 1992. *ADCIRC: An advanced three-dimensional circulation model for shelves coasts and estuaries, report 1: Theory and methodology of ADCIRC-2DDI and ADCIRC-3DL*, Dredging Research Program Technical Report DRP-92-6, U.S. Army Engineers Waterways Experiment Station, Vicksburg, MS, 137p

Luettich, R., and J. Westerink, 2004. *Formulation and Numerical Implementation of the 2D/3D ADCIRC Finite Element Model Version 44.XX.* URL: https://adcirc.org/files/2013/07/adcirc_theory_2004_12_08.pdf.

Macintosh, A., 2013. "Coastal climate hazards and urban planning: how planning responses can lead to maladaptation." *Mitigation and Adaptation Strategies for Global Change* 18, 1035-1055.

Mattupalli, C., Moffet, C., Shah, K., and C.A. Young, 2018. "Supervised classification of RGB aerial imagery to evaluate the impact of a root rot disease." *Remote Sensing*, 6, 917. https://doi.org/10.3390/rs10060917

Meng, X, Currit, N., and K. Zhou, 2010. "Ground filtering algorithms for airborne LiDAR data: a review of critical issues." *Remote Sensing* 2(3), 933-860.

Meyer, M.A., and M.D. Hendricks, 2018. "Using photography to assess housing damage and rebuilding progress for disaster recovery planning." *J. American Planning Association* 84, 127-144.

National Oceanic and Atmospheric Administration — National Weather Service (NOAA-NWS), 2018. Hurricane Michael Wind Swath. Weather Forecast Office Tallahassee, Florida (WFO TAE). Retrieved from: https://www.arcgis.com/home/item.html?id=433fdd370e9046a8bb085924f7617874.

National Hurricane Center (NHC), 2019. "CONUS Hurricane Strike Density (county maps)". Retrieved from: https://www.nhc.noaa.gov/climo/.

National Weather Service (NWS), 2018. Catastrophic Hurricane Michael Strikes Florida Panhandle, October 10, 2018. Retrieved from: https://www.weather.gov/tae/HurricaneMichael2018.

Parece, T.E., and J.B. Campbell, 2015. "Land use/land cover monitoring and geospatial technologies: an overview." *Advances in Watershed Science and Assessment*, The Handbook of Environmental Chemistry 33.

Price, P.E., 2010. "Image analysis with ArcGIS 10." *TerraView,* 54 p.

Ramlal, B., Davis, D., and K. De Bellott, 2018. "A Rapid post-hurricane building damage assessment methodology using satellite imagery." *West Indian Journal of Engineering* 41(1), 74-83.

Rawat, J.S., and M. Kumar, 2015. "Monitoring land use/cover change using remote sensing and GIS techniques: A case study of Hawalbagh block, district Almora, Uttarakhand, India." *The Egyptian Journal of Remote Sensing and Space Sciences* 18(1), 77-84.

Resio, D., Irish, J., and M. Cialone, 2009. "A surge response function approach to coastal hazard assessment — part 1: basic concepts." *Natural Hazards* 51, 163-183.

Robertson, V., W., Zhang, K., and Whitman, D., 2007. "Hurricane-induced beach change derived from airborne laser measurements near Panama City, Florida." *Marine Geology 237,* 191-205.

Simpson, R.H., 1974. "The hurricane disaster-potential scale." *Weatherwise* 27, 169-186.

Stockdon, H., Doran, K.S., and A.H. Sallenger Jr., 2009. "Extraction of lidar-based dune-crest elevations for use in examining the vulnerability of beaches to inundation during hurricanes." *J. Coastal Res.* SI53, 59-65.

Textron Systems Inc. 2017. LiDAR Analyst Extension for ArcGIS. Retrieved from: https://www.textronsystems.com/products/lidar-analyst.

U.S. Census, 2010. "Profile of general population and housing characteristics: 2010 Demographic profile data (DP-1): Mexico Beach city, Florida." American Fact Finder, https://factfinder.census.gov

U.S. Department of Agriculture – National Agriculture Imagery Program (USDA-NAIP). 2017. NAIP Imagery DOQQs, November 2017. Retrieved from: https://www.fsa.usda.gov/programs-and-services/aerial-photography/imagery-programs/naip-qq-and-photocenter-shapefiles/index.

van Aalst, M.K., 2006. "The impacts of climate change on the risk of natural disasters." *Disasters 30(1)*, 5-18.

Viglucci, A., Ovalle, D., Ostroff, C., and N. Nehamas, 2018. "Florida's building code is tough but Michael was tougher. Is it time for a rewrite?" *Miami Herald.* Retrieved from: https://www.miamiherald.com/news/state/florida/article219862625.html

Zakaluk, R., and R.S. Ranjan, 2008. "Predicting the leaf water potential of potato plants using RGB reflectance." *Canadian Biosystems Engineering*, 7.1.

Zhang, K., Whitman, D., Leatherman, S., and W. Robertson, 2005. "Quantification of beach changes caused by Hurricane Floyd along Florida's Atlantic coast using airborne laser surveys." *J. Coastal Res.* 21(1), 123-134.

Zhou, Z., and J. Gong, 2018. "Automated analysis of mobile LiDAR data for component-level damage assessment of building structures during large coastal storm events." *Computer-Aided Civil and Infrastructure Engineering* 33, 373-392.